



Low-Cycled Hysteresis Characteristics of Circular Hollow Steel Damper Subjected to Inelastic Behavior

Daniel Y. Abebe¹ · Jin Woo Kim² · Gyumyong Gwak³ · Jae Hyouk Choi⁴

Received: 30 September 2016 / Accepted: 5 June 2018 / Published online: 9 July 2018
© The Author(s) 2018

Abstract

This study aims to evaluate hysteresis response behavior of circular hollow steel damper (CHSD). Steel dampers are a type of passive dampers and commonly used for seismic dissipation in civil engineering structures. Steel dampers are widely used for seismic energy dissipation because they are easy to install, maintain and they are also inexpensive. CHSD is among steel dampers which dissipates seismic energy through metallic deformation and geometrical elasticity of circular shape and fatigue resistance around welded connection to the end plates. Finite element analysis was conducted in order to evaluate the hysteresis characteristics and low cycle fatigue behavior of CHSD using failure index. To verify the analysis simulation quasi static loading was conducted and the result was compared and satisfactory result was obtained.

Keywords Hysteresis characteristics · Circular hollow steel damper · Aspect ratio · Quasi-static loading · Large deformation · FE analysis

1 Introduction

Damage control design concept for civil engineering structures have been widespread to mitigate hazards caused by earthquake since 1995, Kobe, Japan earthquake disaster (Nakashima et al. 1994). Over the same period, after the 1995 Hyogo-ken Nanbu earthquake, structural control has paid much attention to seismic design, with the premise that such control can improve ultimate resisting capacity of structures and reduce damage during earthquake (Tadaki et al. 2000). There are a number of methods to improve the resisting capacity and reduce the damages during earthquakes. Hysteretic steel damper is a passive damper system that absorbs substantial portion of input energy induced by earthquake through hysteretic deformation of the damper material. A number of innovative hysteretic steel dampers with

high energy dissipation capacity have been developed and/or proposed and evaluated in the past 20 years. Some of the hysteretic steel dampers developed and evaluated includes: Buckling resistance steel damper (Jeong et al. 2016; Deng et al. 2015), shear panel damper (Abebe et al. 2014), Circular shear panel damper (CSPD) (Abebe et al. 2014), Tadas device (Yeh et al. 2004), steel plate added damping and stiffness (ADAS) (Hanson et al. 1992), slit steel damper (Ricky et al. 2008). Some of the details of these devices are presented in Fig. 1. The hysteresis behavior and failure mode under cyclic loading of these dampers are also different.

Circular hollow steel damper is a type of steel damper as the name also indicates and dissipates seismic energy mainly through inelastic deformation or through hysteretic material. Under cyclic loading the circular shape of circular hollow steel damper (CHSD) changed to elliptical shape which gives CHSD an extra energy absorbing capacity. Among steel dampers such as shear panel damper CHSD has an advantage of resisting applied load in all direction. Thus, because of its circular shape CHSD in the practical situation can resist loads in all direction which is advantageous since the action of force during earthquake is multi-dimensional. (Abebe and Choi 2012). Abebe et al. (2013), studied the effect of aspect ratio of CHSD using simple engineering mechanics (de Souza Neto et al. 2008) and found that the effective aspect ratio of CHSD is:

✉ Jae Hyouk Choi
jh_choi@chosun.ac.kr

¹ Smart Green Construction Technology Research Center, Chosun University, Gwangju 501-759, Korea

² Osaka University, Osaka 565-0871, Japan

³ Samoo Structural Consultants Co., Seoul 04799, Korea

⁴ School of Architectural Engineering, Chosun University, Gwangju 501-759, Korea

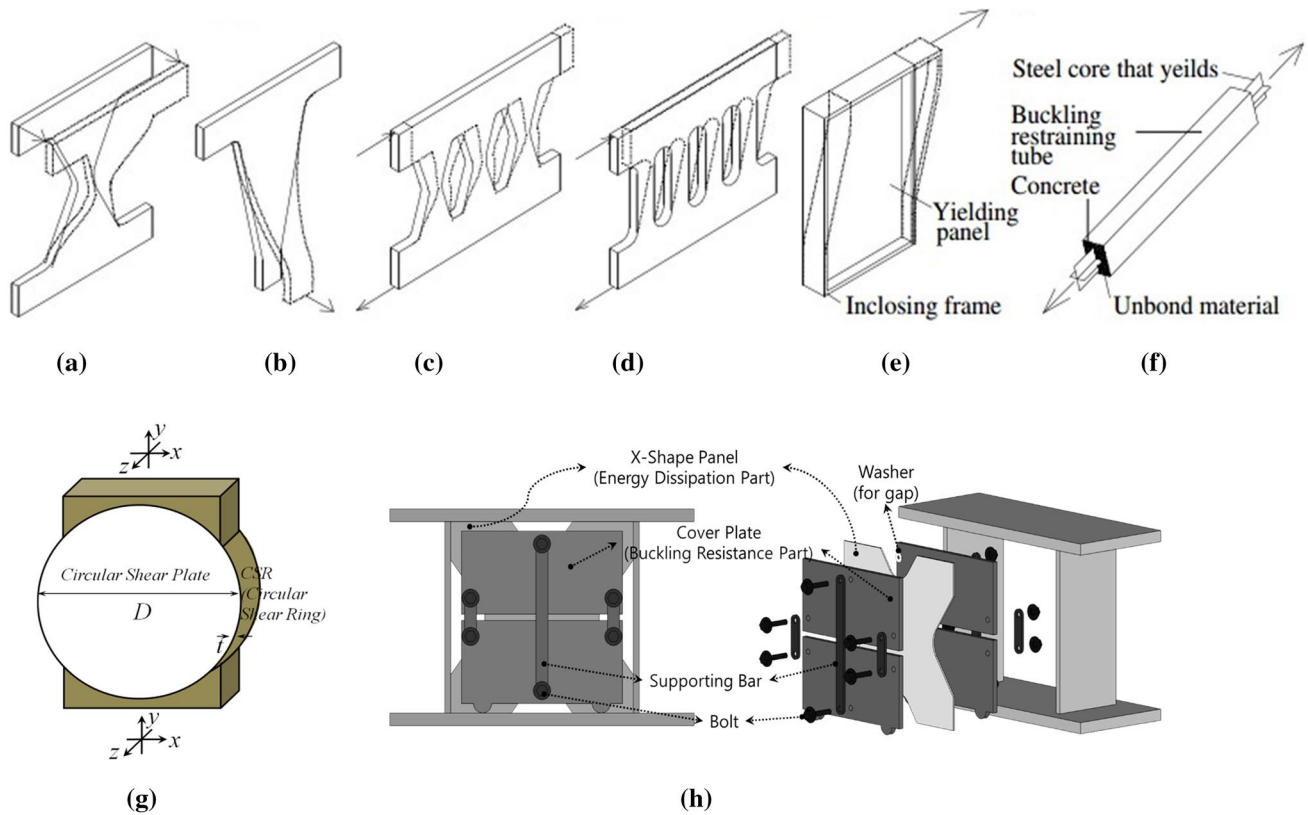


Fig. 1 Types of metallic dampers: **a** ADAS; **b** TADAS; **c** honeycomb damper; **d** slit damper; **e** shear panel damper; **f** buckling restrained brace; **g** circular shear panel damper; **h** buckling resistance steel damper

$$\frac{h}{r} = \frac{H}{D} = \sqrt{3} \tag{1}$$

where H and D is the height and diameter of CHSD respectively and the details of these variables are shown in Fig. 2. This aspect ratio is taken as effective CHSD where both bending and shear stresses resisted and it also satisfies the von Mises’s yield stress criteria. The failure mode of CHS damper is different depending on the height to diameter ratio. Specimen having H/D greater than $\sqrt{3}$ the failure is bending failure and the failure for specimen having H/D less than $\sqrt{3}$ is shear failure (Abebe and Choi 2012).

CHSD can be considered as a fixed ended beam and the corresponding bending stress and shear stress distribution on the cross-section is shown in Fig. 3a, b respectively. The stress distribution both bending stress and shear stress on the infinitesimal length of CHSD is presented in Fig. 3c. The detail of specimen is shown in Fig. 4 and finite element analysis was conducted for grasping the hysteresis response and low cycle fatigue behavior of hollow section steel damper having aspect ratio of $\sqrt{3}$. To confirm the validity of the finite element analysis conducted, the comparison between test result and analysis result was undertaken. The deformation mode, hysteresis response and cumulative dissipated

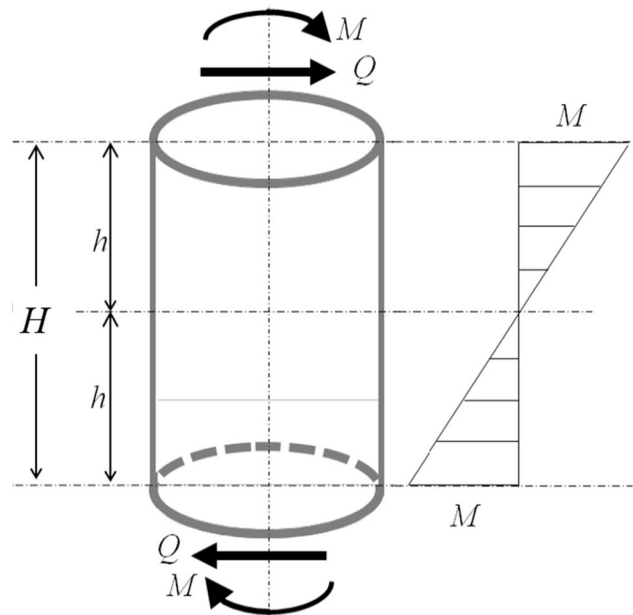


Fig. 2 Loading condition of CHSD
energy of selected CHSD was compared. Diameter-to-thickness (D/t) ratio is the main parameter considered in non-linear FE analysis. The low cycle fatigue of analysis

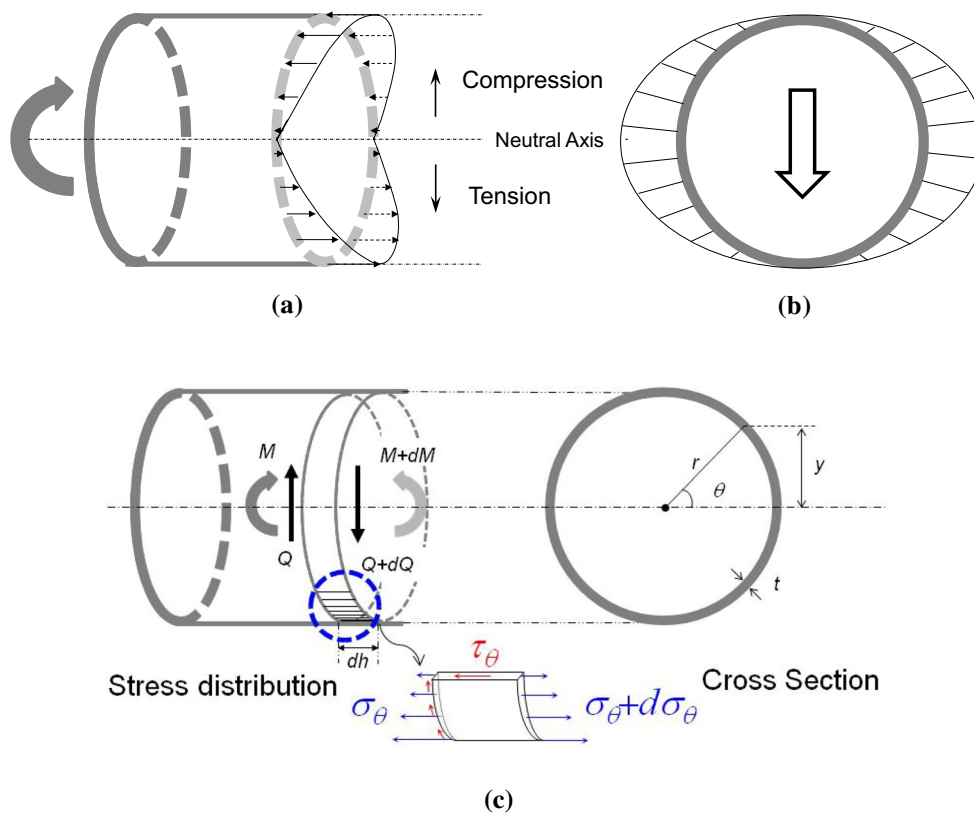


Fig. 3 Stress distribution on CHS damper. **a** Bending stress distribution, **b** shear stress distribution, **c** stress distribution on the infinitesimal length

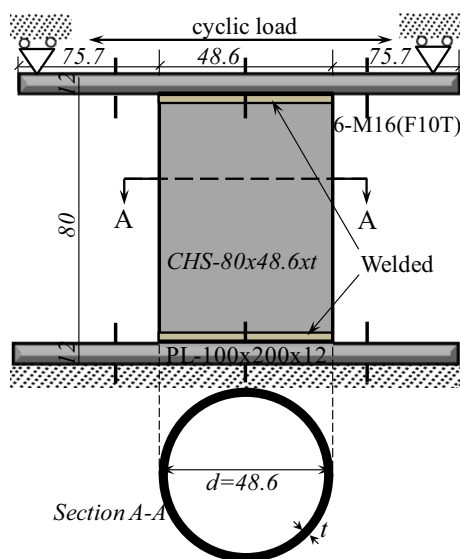


Fig. 4 Specimen detail and boundary conditions

specimens was evaluated using PEEQ index and section with low PEEQ index was identified.

2 Non-linear Finite Element Analysis

Circular hollow steel damper was discretized using a three dimensional finite element analysis model called ABAQUS package to evaluate the hysteresis characteristics and low cycle fatigue behavior of CHS damper (ABAQUS ver. 6.10-1 2011). Material nonlinearity was included in the finite element model by specifying a stress–strain curve in terms of the true stress and true strain as shown in Fig. 5. The engineering stresses and strains obtained from the coupon tests were converted into true stresses and strains for this purpose using Eqs. (2) and (3) respectively. Both solid and shell element model have been tried in order to choose the suitable element to simulate the hysteresis behavior. A 3-D shell element S4R quadrilateral elements through mesh generation by Python script is found to be more efficient in modeling CHS damper with linear interpolation and reduced integration are used, as shown in Fig. 6. The structural steel components are modeled as an elastic–plastic material. With elastic and plastic options, the yield and ultimate tensile strength obtained firstly from the results of the coupon tests and then converted into the true stress and plastic strain with appropriate input format for ABAQUS. In the plastic range the important behavior of structural steel to be

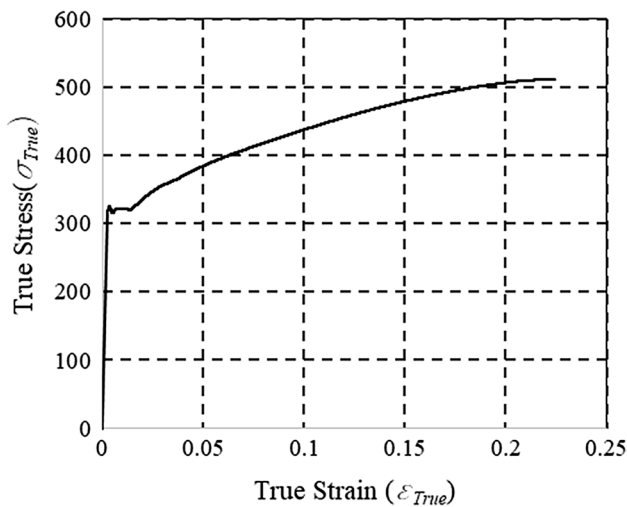


Fig. 5 True stress–true strain curve

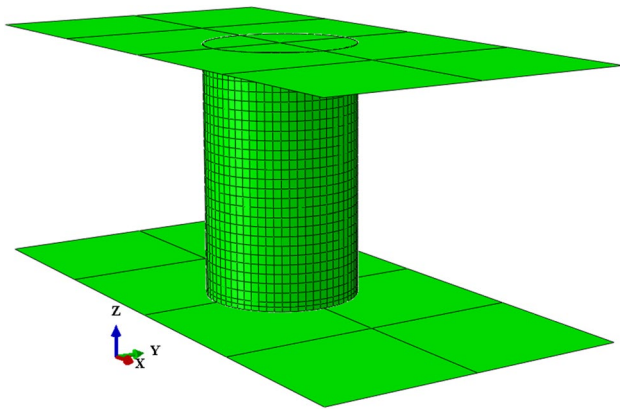


Fig. 6 3D-Meshed analysis Model

considered is strain hardening behavior. Strain hardening is a phenomenon which results in an increase in hardness and strength of a metal subject to plastic deformation (cold working) at temperatures lower than the recrystallization range. Among commonly used strain hardening model in Abaqus, combined hardening i.e. combined isotropic and kinematic hardening model was used. Different mesh sizes have been examined as well to determine a reasonable mesh that provides both accurate results with less computational time. The exam results show that, if the mesh is too coarse, a convergence problem will be caused as the contact element was used between the circular hollow section and the endplate surface. However, if the mesh is too fine, the computational time is excessive. Each ends of the components are created a more refined mesh as shown in Fig. 6 because of those areas were where most stresses are concentrated and is the area exposed direct compression and tension forces.

$$\sigma_{tr} = \sigma_e(1 + \epsilon_e) \quad (2)$$

$$\epsilon_{tr} = \ln(1 + \epsilon_e) \quad (3)$$

where σ_{tr} : true stress, σ_e : engineering stress, ϵ_{tr} : true strain, ϵ_e : engineering strain. The true yield stress, ultimate stress and strain of a specimen taken from CHSD having thickness 3.2 mm and flattened are 321 MPa, 511 MPa and 22.38% respectively.

3 Constraint and Loading Condition

The boundary conditions are controlled at the reference points created at the center both end plates. All the translational and rotational displacement components are fixed at the reference points of the lower end plate. A cyclic load was given at upper end plate reference points in X-direction fixing all the translation and rotation in other direction. The boundary condition and method of loading adopted in the finite element analysis followed to have the specimen shear effect and the same as those used in the tests for verification. A constant strain loading is implemented in which the load is applied by controlling the displacement with the displacement protocol shown in Fig. 8.

4 Verification of Finite Element Analysis

4.1 Test Set-Up and Process

In order to verify the analysis model a quasi-static loading test was carried out. The test set-up and general equipment system is shown in Fig. 7 to evaluate the specimen detailed in Fig. 4 having thickness 3.2 mm (CHS80×48.6×3.2). In this the test set-up, to avoid rotation angle on the top of specimen pantograph was installed and counter weight installed using a principle of a pair of scale was arranged to protect axial force supposed to be applied on the test specimen. Displacement meters for measuring deformation of circular hollow steel dampers were installed at the top end plate and the bottom end plate of the experiment specimen. The difference between displacements measured at the top end plate and bottom end plate was taken as the shear displacement. The force response of specimen was measured directly from the load cell mounted on the actuator. The cyclic loading proceeds up to final failure and the loading is applied by controlling the displacement following the loading condition used in finite element analysis. The displacement protocol used for experiment is the same as the protocol used in the analysis model which is shown in Fig. 8.

4.2 Comparison of Results

The comparison of deformation mode of test and analysis result of CHS damper using conventional mild steel (SS400)

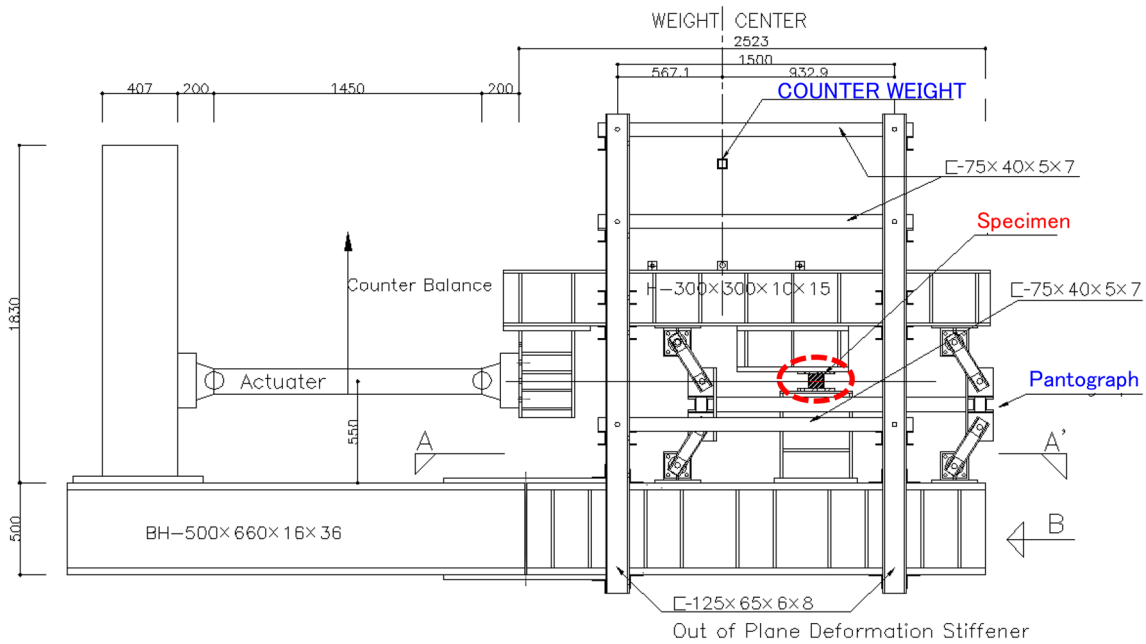


Fig. 7 Loading equipment system

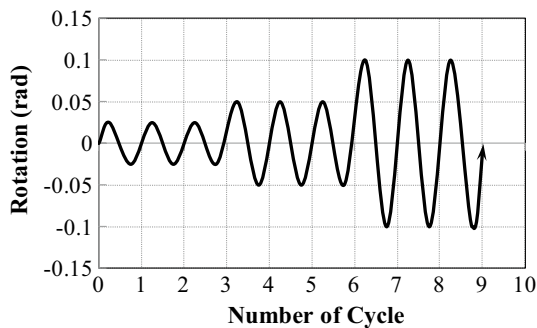


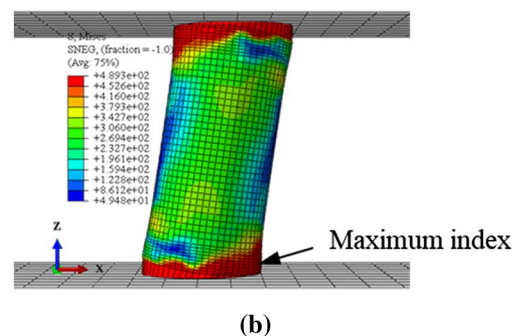
Fig. 8 Loading protocol

is presented in Fig. 9. The small cracks was observed on the test specimen. In addition, the circular shape of both test and analysis specimen changed to elliptical shape under large displacement which gives circular hollow section damper advantage over other steel damper. The deformation mode with von Mises stress distribution is plotted at the same maximum loading with the test specimen. The stress concentration is high at both ends in the loading direction. The maximum stress is also observed at lower ends in the direction of loading as indicated in Fig. 9b.

The hysteresis response of analysis and test results were also compared. Looking at the shear force-inelastic rotation graphs presented on Fig. 10, there is no apparent difference between the quasi static test result and FE simulation results. Which shows that finite element analyses accurately evaluates the failure mode, hysteresis characteristics and



(a)



(b)

Fig. 9 Comparison of deformation mode of test result and von Mises stress distribution of analysis result. a Test result, b analysis result

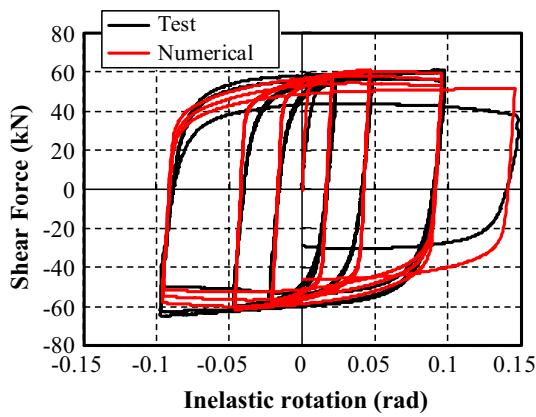


Fig. 10 Comparison of shear force-inelastic rotation relationship

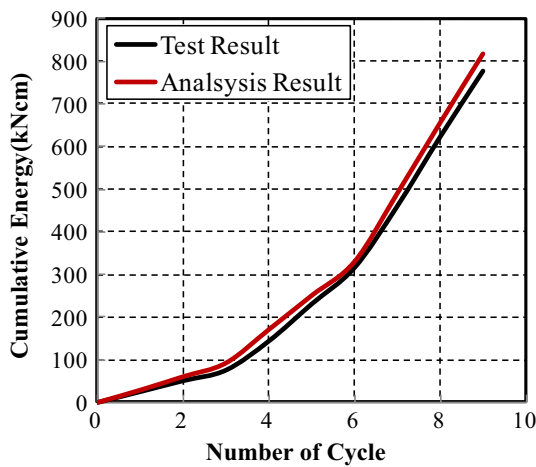


Fig. 11 Cumulative energy versus number of cycle

the performance of CHS damper. In the plotted graph, the black solid line represents experimental result and the red line shows the analysis result. The strength degradation of test specimens are faster than analysis specimens. This effect is observed in the comparison of cumulative energy plotted with respect to number of cycles shown in Fig. 11. Cumulative energy dissipation is the sum of the energy dissipation for each cycle, i , up to the maximum number of cycles being considered, N , presented in Eq. (4) below. As shown in the Fig. 11 the cumulative energy calculated from the hysteresis curves presented in the Fig. 11, the analysis results shown a slight bigger cumulative energy compared to the results obtained from experiments.

$$E_T = \sum_{i=1}^N \left(\int QHd\gamma \right)_i \tag{4}$$

where Q is the shear force and $Hd\gamma$ is the end plastic shear deformation written as the product of the incremental link rotation, $d\gamma$, times the height of CHS damper H .

4.3 Low Cycle Fatigue Failure

Recent analytical studies of steel frame components have used a low cycle fatigue failure index based on a stress modified critical strain criterion. The failure in numerical simulation can also be predicted by the failure index in addition to the strength reduction in hysteresis response. The failure index is defined by the triaxiality of the stress field and the accumulated plastic strain in tension and compression (Hancock and Mackenzie 1976; McClintock 1968). The objective function is the dissipated energy before failure of the damper. The ductility capacity of the damper is defined using failure index as follows. The variables, which are functions of pseudo-time, such as stresses and strains are evaluated at integrated maximum possible point. Let $\epsilon_p(t)$ denote the equivalent plastic strain defined as:

$$\epsilon_p(t) = \int_0^t \dot{\epsilon}_{ij}^p(t) \dot{\epsilon}_{ij}^p(t) dt \tag{5}$$

where $\epsilon_{ij}^p(t)$ is the plastic strain tensor, (\cdot) is the derivative with respect to time, and the summation convention is used. The equivalent plastic strain represents amount of plastic deformation in material level, and is evaluated at each integration point. Many fracture criteria have been presented using $\epsilon_p(t)$. We use an extended version of the SMCS criterion that was developed for simulating ductile fracture of metals due to void growth. The critical plastic strain ϵ_{cr} is first defined as:

$$\epsilon^{cr} = \alpha \exp -1.5 \frac{\sigma_m}{\sigma_e} \tag{6}$$

where σ_m is the mean stress, and σ_e is the von Mises equivalent stress given by Eqs. (7) and (8), respectively. The parameter α is dependent on material. Equation (6) indicates that the critical plastic strain for ductile fracture depends on the stress triaxiality σ_m/σ_e . Then the failure index for monotonic loading is defined as in Eq. (9) (Oh et al. 2011).

$$\sigma_m = \frac{\sigma_1 + \sigma_2 + \sigma_3}{3} \tag{7}$$

$$\sigma_e = \sqrt{\frac{1}{2} [(\sigma_1 - \sigma_2)^2 + (\sigma_1 - \sigma_3)^2 + (\sigma_2 - \sigma_3)^2]} \tag{8}$$

$$I_f = \frac{\epsilon_p}{\epsilon^{cr}} \tag{9}$$

The material is assumed to fracture when I_f reaches 1.0. The Eqs. (5) and (8) are based on the ductile fracture due to void growth under monotonic tensile deformation. However, we need the effect under cyclic loading, where the void

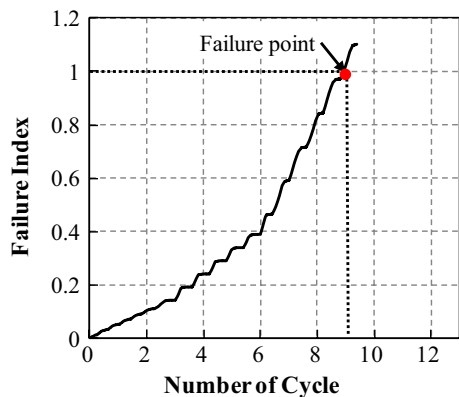


Fig. 12 Failure index versus number of cycle

shrinks due to compressive plastic loading. Therefore, the following formulation by Kanvinde and Deierlein is used (Chi et al. 2006; Mackenzie et al. 1977). The equivalent plastic strain ϵ_p is divided into tensile plastic loading states ϵ_t (> 0) and compressive plastic loading states ϵ_c (> 0), which are identified by the sign of σ_m . The significant plastic strain ϵ^* , which represents the amount of void growth, is defined as (Ohsaki and Nakajima 2012):

$$\epsilon^* = \epsilon_t - \epsilon_c \tag{10}$$

The critical value ϵ^{cr*} for ϵ^* is given as:

$$\epsilon^{cr*} = \exp(-\lambda\epsilon_p)\epsilon^{cr} \tag{11}$$

where λ is a positive material parameter and according to Kanvinde and Deierlein the parameter λ for the failure index may vary between 2.5 and 8.0. In the following, an intermediate value 4.3 is used for λ . Ductile fracture is assumed to occur when the cyclic failure index I_f^* , defined as follows, reaches 1.0:

$$I_f^* = \frac{\epsilon^*}{\epsilon^{cr*}} \tag{12}$$

Figure 12 shows failure index versus number of cycle relationship of analysis result measured at indicated maximum failure index in Fig. 9b. From the figure CHS damper was fractured at the 9.21th cycle. The failure index described in Eq. (9) reasonably predict fracture initiation under monotonic loading, but is less accurate for cyclic loading. Kanvinde and Deierlein (2004) showed on average, 10% agreement between the fracture criterion and monotonic coupon tests. However compared to the simple method of determining the fracture in numerical simulation which is strength degradation under cyclic load loading, the fracture predicted by the failure index calculated using Eq. (12) is more accurate.

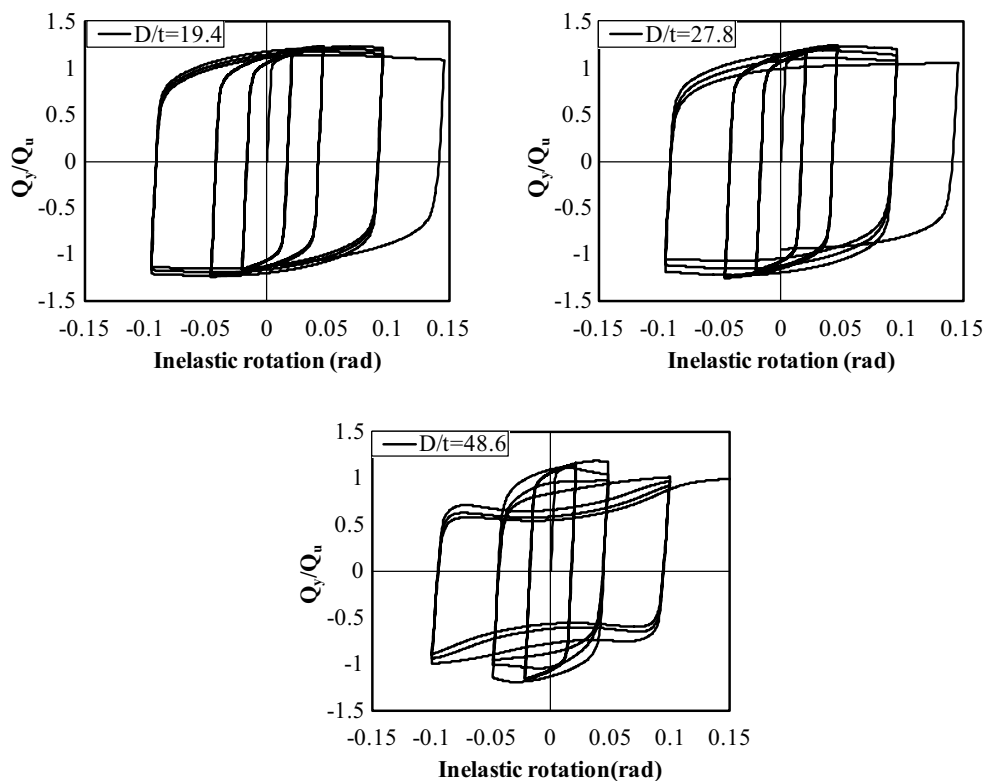


Fig. 13 Shear force and inelastic rotation relationships

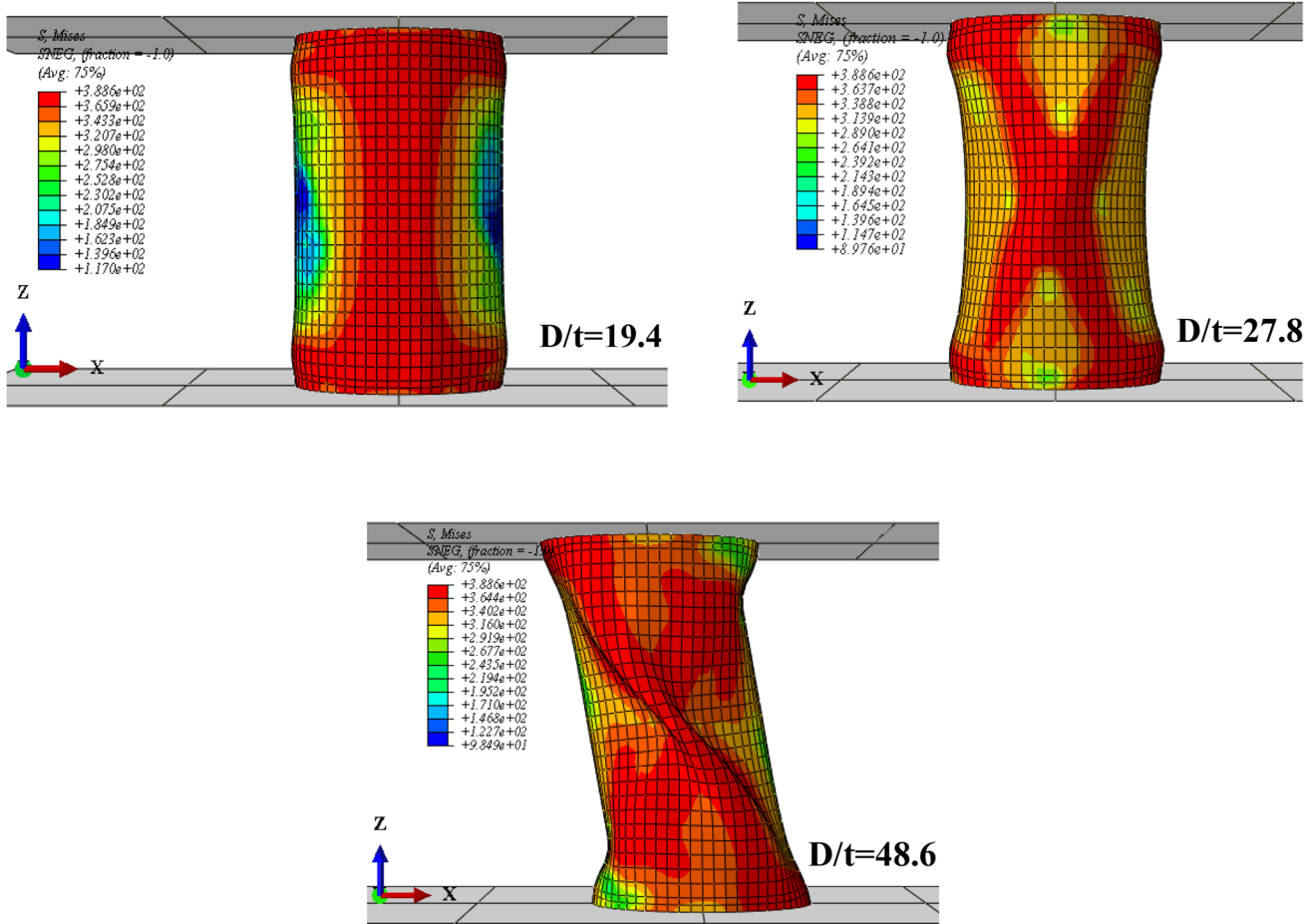


Fig. 14 Deformation mode and von Mises’s stress distribution of analysis result

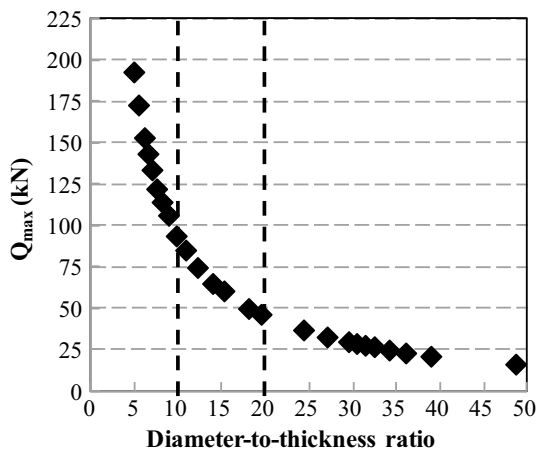


Fig. 15 Maximum shear force versus d/t ratio

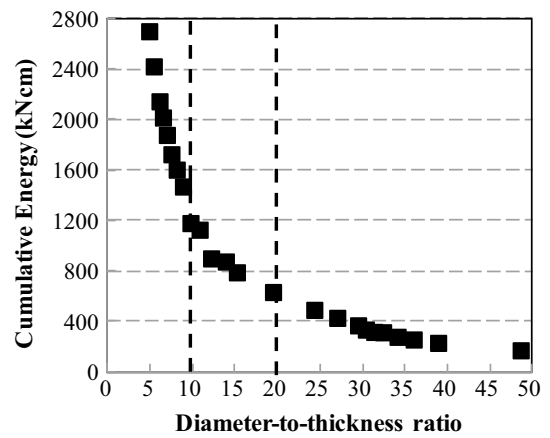


Fig. 16 Cumulative energy versus d/t ratio relationship

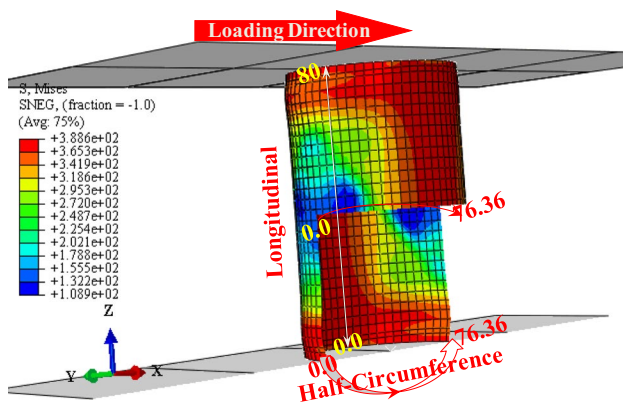


Fig. 17 PEEQ measurement location

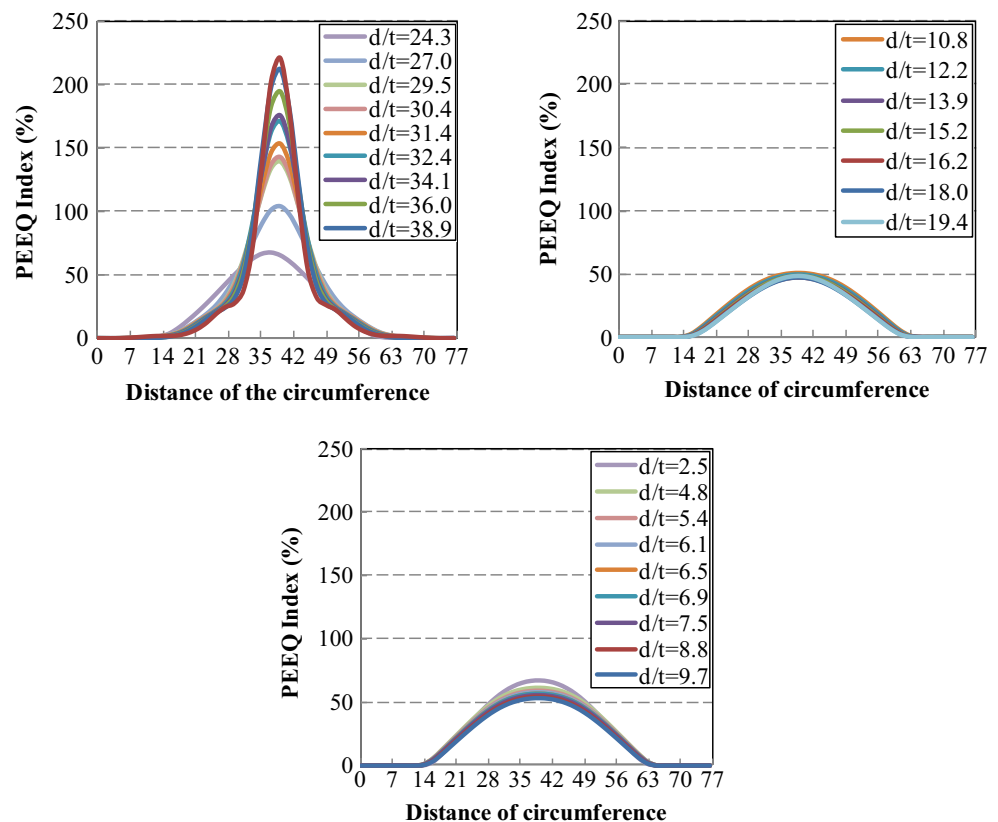
4.4 Effect of Diameter-to-Thickness Ratio

To extend the evaluation on circular hollow steel damper, the effect of diameter-to-thickness ratio is studied analytically. Generally three different buckling and hysteresis characteristics are found. First, specimen having $D/t < 19.4$, which can be taken as a compact section, in which yielding prior to buckling without strength degradation is observed. The second type is the specimen having a diameter-to-thickness ratio of $19.4 \leq D/t \leq 27.8$ that yielding prior to buckling with strength degradation is noticed. The final type is

diameter-to-thickness ratio of $D/t > 27.8$ where yielding with buckling and strength degradation which forms pinching at initial displacement. The hysteresis loops of these three behavior of CHS-damper is presented in Fig. 13. The corresponding deformed shape with von Mises's stress distribution approximately taken at 9.21th cycle, where the fracture is occurred, is presented in Fig. 14 for analysis specimens having $D/t = 19.4, 27.8$ and 48.6 . As shown in the figure, the buckling mode as well as the stress distribution is different for different D/t ratio. Analysis specimen having $D/t = 19.4$, shows stable hysteresis response and severe buckling shape wasn't occurred unlike analysis specimen having $D/t = 48.6$ where unstable hysteresis response and severe buckling was observed. The pinching formed for $D/t > 27.8$ is also due to out-of-plane buckling of the circular hollow section under cyclic loading.

The maximum shear force for all considered analysis specimen is summarized in Fig. 15. As shown in the Fig. 15, the maximum shear force decreases with an increase of diameter-to-thickness ratio. Cumulative energy can be calculated from the hysteresis curves for all analysis specimens considered using Eq. (4). The plot of cumulative energy versus the diameter-to-thickness ratio is shown in Fig. 16. The behavior of cumulative energy is similar to that obtained for maximum shear force where cumulative energy decreases with an increase of diameter-to-thickness ratio.

Fig. 18 PEEQ index measured in half circumference



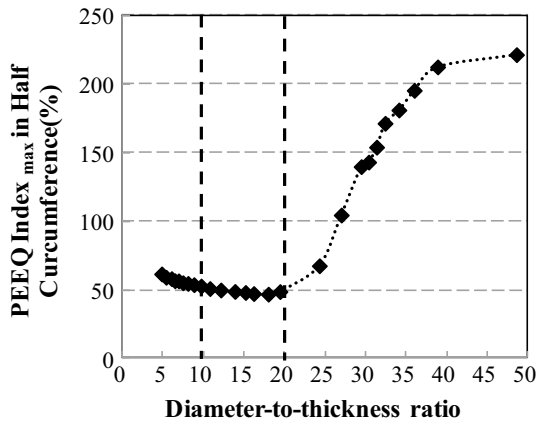


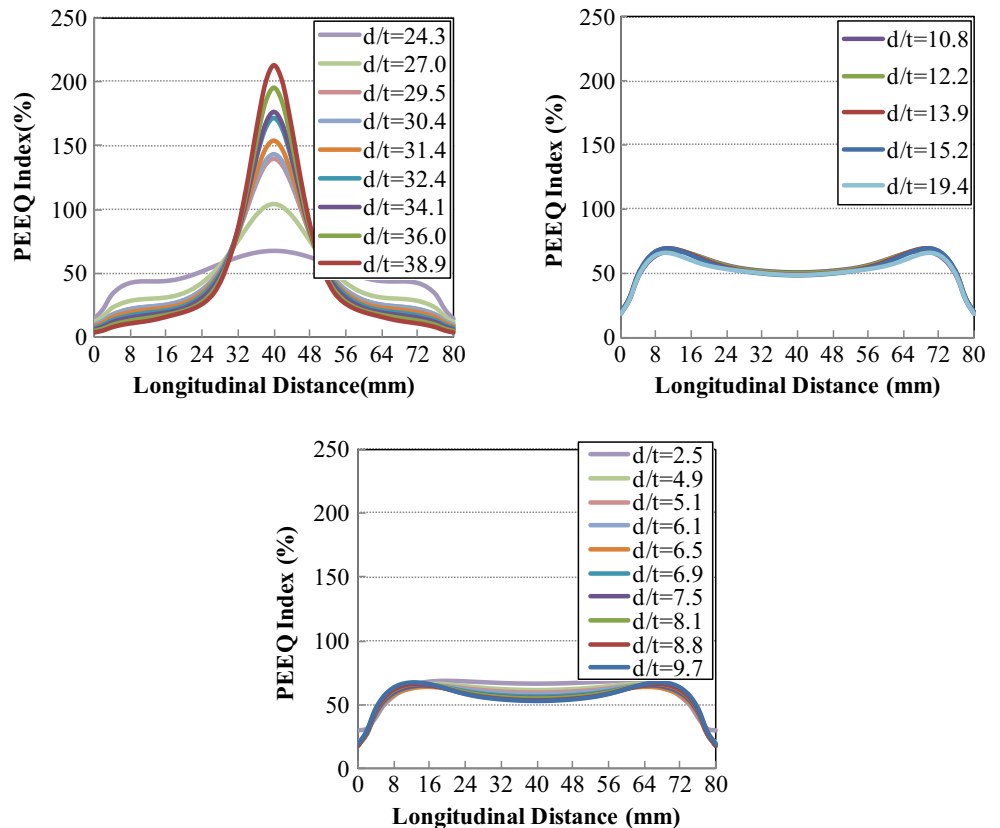
Fig. 19 Circumference PEEQ index—d/t relationship

In order to evaluate the effect of diameter-to-thickness ratio on low fatigue failure behavior of circular hollow section damper a using simple approaches called PEEQ Index. The PEEQ Index is given by the ratio of the plastic equivalent strain to the yield strain.

$$PEEQ\ Index = \frac{\epsilon_e^p}{\epsilon_y} \tag{13}$$

where ϵ_e^p : is the equivalent plastic strain and ϵ_y : yield strain which is given by the ratio of yield strength to young’s modulus (σ_y/E) and the calculated yield strain is approximately 0.002. The equivalent plastic strain was measured around half circumference at middle of the specimen at each node starting from the direction of loading and longitudinally as shown in the section in Fig. 17. The calculated maximum equivalent plastic strain index (PEEQ Index) at each node around the circumference for the parametrical study of analysis specimens (diameter-to-thickness ratio) with the respect to circumference distance is presented in Fig. 18. The circumference distance is measured taking in the loading direction, form extreme compression to extreme tension under cyclic loading. The peak PEEQ Index presented in Fig. 18 are plotted with respect to D/t ratio as shown in Fig. 19. In the way, PEEQ Index measured and calculated at each nodes in longitudinal direction for all analysis specimens is presented in Fig. 20. The peak values PEEQ Index for each analysis specimens also plotted with respect to D/t ratio as shown in Fig. 21. The peak PEEQ Index values calculated in both half circumference and longitudinal direction plotted against D/t ratio forms S-shape curves, Figs. 19 and 21. The lowest PEEQ Indexes can be taken as effective section in CHSD. Thus, from Figs. 19 and 21, D/t ratio between 10 and 20 are the effective cross-section of CHSD.

Fig. 20 PEEQ index measured longitudinally



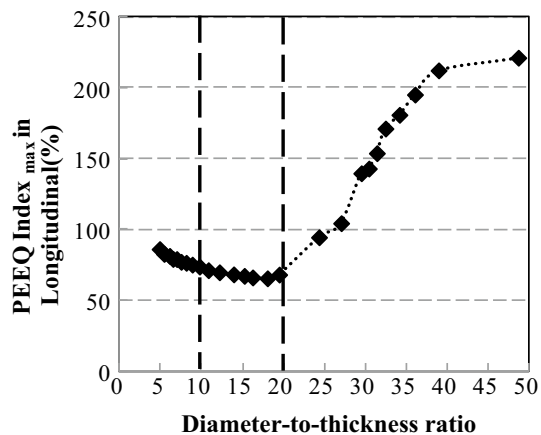


Fig. 21 Longitudinal PEEQ index—d/t relationship

5 Conclusion

The hysteresis and low fatigue failure behavior of circular hollow section steel damper was evaluated through non-linear finite element and the analysis is of course verified by quasi-static loading test and the following conclusion was drawn.

Depending on the diameter-to-thickness ration (D/t) the hysteresis response as well as the buckling mode of circular hollow section steel damper is different. It is found that, thin CHSD, $D/t > 27.8$, the hysteresis response forms pinching at initial displacement and severe out-of-plane buckling was also observed. As the thickness increase the hysteresis response became stable. The low cycle fatigue behavior is evaluated using failure index and PEEQ index. The failure index for CHS80×48.6×3.2 reaches 1 at 9.21th cycle where the cyclic load resisting strength started to degrade for both analysis and test results. The diameter-to-thickness parameter considered the PEEQ index in longitudinal and half the circumference. The minimum PEEQ index is found for D/t ratio between 10 and 20. This section can be taken as the effective section for circular hollow section damper.

Acknowledgements This work was financially supported by Basic Science Research Program through the National Research Foundation of Korea (NRF) funded by the Ministry of Education, Science and Technology (No. 2015-053557) and supported by research fund from Chosun University, 2016.

Open Access This article is distributed under the terms of the Creative Commons Attribution 4.0 International License (<http://creativecommons.org/licenses/by/4.0/>), which permits unrestricted use, distribution, and reproduction in any medium, provided you give appropriate credit to the original author(s) and the source, provide a link to the Creative Commons license, and indicate if changes were made.

References

- ABAQUS ver. 6.10-1. (2011). *User manual and documentation*. Providence: Dassault Systems.
- Abebe, D. Y., & Choi, J. H. (2012). Structural performance evaluation on circular pipe steel damper. In *Proceedings of international union of materials research society—international conference in Asia*.
- Abebe, D. Y., Jeong, S. J., Getahun, B. M., Segu, D. Z., & Choi, J. H. (2014). Study on hysteretic characteristics of shear panel damper made of low yield point steel. *Materials Research Innovations*, 19(S5), S5-902–S5-910.
- Abebe, D. Y., Kim, J. W., & Choi, J. H. (2013). Hysteresis characteristics of circular pipe steel damper using LYP225. In *Proceedings of Steel Innovation conference, February, 22–26, Christ Church, New Zealand*.
- Chi, W. M., Kanvinde, A. M., & Deierlein, G. G. (2006). Prediction of ductile fracture in steel connections using SMCS criterion. *Structural Engineering*, 132(2), 171–181.
- de Souza Neto, E. A., Perić, D., & Owen, D. R. J. (2008). *Computational methods for plasticity: Theory and applications*. New York: Wiley.
- Deng, K., Pan, P., Li, W., & Xue, Y. (2015). Development of a buckling restrained shear panel damper. *Journal of Constructional Steel Research*, 106, 311–321.
- Hancock, J. W., & Mackenzie, A. C. (1976). On the mechanics of ductile failure in high-strength steel subjected to multi-axial stress-states. *Journal of the Mechanics and Physics of Solids*, 24, 147–160.
- Hanson, R. D., Xia, C., & Su, Y. F. (1992). Design of supplemental steel damping devices for buildings. In *Proceedings of the 10th world congress on earthquake engineering, Balkema, Rotterdam*.
- Jeong, S. J., Abebe, D. Y., Gwak, G. Y., & Choi, J. H. (2016). Analytical evaluation of buckling resistance steel damper. In *Proceedings of the 7th international conference on computational methods, August 1–4, Berkeley, CA, USA*.
- Kanvinde, A. M., & Deierlein, G. (2004). *Micromechanical simulation of earthquake induced fracture in steel structures*. Tech. Rep. TR145, Blume Center, Stanford University.
- Mackenzie, A., Hancock, J., & Brown, D. (1977). On the influence of state of stress on ductile failure initiation in high strength steels. *Engineering Fracture Mechanics*, 9, 167–188.
- McClintock, F. A. (1968). A criterion of ductile fracture by the growth of holes. *Journal of Applied Mechanics*, 35(2), 363.
- Nakashima, M., Iwai, S., Iwata, M., Takeuchi, T., Konomi, S., Akazawa, T., et al. (1994). Energy dissipation behaviour of shear panels made of low yield steel. *Earthquake Engineering and Structural Dynamics*, 23(12), 1299–1313.
- Oh, C. S., Kim, N. H., Kim, Y. J., Baek, J. H., Kim, Y. P., & Kim, W. S. (2011). A finite element ductile failure simulation method using stress-modified fracture strain model. *Engineering Fracture Mechanics*, 78(1), 124–137.
- Ohsaki, M., & Nakajima, T. (2012). Optimization of link member of eccentrically braced frames for maximum energy dissipation. *Journal of Constructional Steel Research*, 75, 38–44.
- Ricky, W. C., & Faris, A. (2008). Experimental study of steel slit damper for passive energy dissipation. *Engineering Structure*, 30(4), 1058–1066.
- Tadaki, K., Shigeki, I., Hisaya, K., Takuya, U., & Haruhito, O. (2000). Experimental study on hysteresis damper with low yield strength steel under dynamic loading. In *Proceedings of 12th World Congress on Earthquake Engineering, Auckland, New Zealand*.
- Yeh, C. H., Lu, L. Y., Chung, L. L., & Huang, C. S. (2004). Test of a full-scale steel frame with TADAS. *Earthquake Engineering and Engineering Seismology*, 3(2), 1–16.